JCBI
Journal of Computing & Biomedical Informatics
ISSN: 2710 - 1606
Volume 10 Issue 02
2026

Research Article
https://doi.org/10.56979/1002/2026/1234

Stress Detection from Photoplethysmography Signals Using Multi-Domain Heart Rate Variability Analysis

Wadeea Alnufaily[1], Ramasamy Srinivasagan[1*], Purushothaman R[2], and Mohammed Alnaeem[1]

[1]Computer Engineering, College of Computer Science and Information Technology, Al Ahsa, 36362, Saudi Arabia.
[2]Nano Electronics System, TU Dresden, 01062, Germany.
[*]Corresponding Author: Ramasamy Srinivasagan. Email: rsamy@kfu.edu.sa

Received: November 21, 2025 **Accepted:** February 12, 2026

Abstract: Stress is a key contributor to cardiovascular and mental health disorders, which motivates reliable, non intrusive monitoring methods for early detection and intervention. Photoplethysmography (PPG) has emerged as a practical alternative to electrocardiography (ECG) for wearable cardiovascular monitoring because of its low cost and ease of integration into consumer devices. This study presents a stress detection framework based on multi domain pulse rate variability (PRV) analysis derived from PPG signals. Publicly available datasets, including the Wearable Stress and Affect Detection (WESAD) dataset and a Pulse Transit Time (PTT) PPG dataset, are used to validate the proposed signal processing and feature extraction pipeline. Raw PPG signals are preprocessed with bandpass filtering and robust peak detection to obtain inter beat intervals, from which time domain, frequency domain, and nonlinear PRV features, as well as the Baevsky Stress Index, are computed. On WESAD, statistically significant differences between baseline and TSST induced stress conditions are observed in key PRV features (e.g., SDNN, RMSSD, pNN50, LF/HF ratio, SD1, SD2, ApEn, SampEn; Bonferroni corrected $p < 0.0029$), indicating reduced variability, a shift toward sympathetic dominance, and decreased dynamical complexity during stress. A subset of features also shows strong stability across window lengths from 2 to 5 minutes ($R^2 \geq 0.6$ when compared to 5 minute reference segments), supporting their use in near real time monitoring. These results confirm the feasibility of PPG based, multi domain PRV analysis for non invasive stress assessment and highlight its suitability for wearable and edge based healthcare applications.

Keywords: Photoplethysmography; Pulse Rate Variability; Stress Detection; Heart Rate Variability; Wearable Sensor; Baevsky Stress Index

1. Introduction

Stress has become an increasingly widespread health fear in modern community, with chronic exposure contributing to cardiovascular diseases (CVDs), metabolic disorders, and mental health conditions. According to global health statistics, cardiovascular diseases remain the most cause of mortality worldwide, calculating for millions of deaths every year [1-3]. Psychological and physiological stress directly influences autonomic nervous system (ANS) regulation, leading to altered cardiac rhythm, vascular tone, and reduced adaptive capacity of the cardiovascular system. Consequently, reliable stress monitoring plays a big role to prevent healthcare and long-term disease management. Numerous successful methods for lowering cardiovascular (CV) risk have been described, including pharmacological therapies like anticoagulants, lipid-altering medications, and antihypertensive drugs, as well as lifestyle changes like regular exercise, better eating habits, and weight control [4]. Heart Rate Variability (HRV) is a typically used technological biomarker for both of the parasympathetic and sympathetic autonomic nervous systems [5]. Fig 1. depicts the Autonomic Nervous System Pathway.

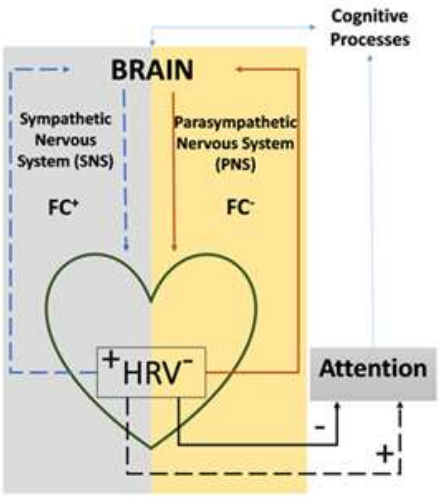

Figure 1. Autonomic Nervous System Pathway

Sample entropy (SampEn) and compared it to approximate entropy (ApEn) on simulated signals and physiological time series, including RR-interval data, varying record lengths and noise levels. The SampEn reduced bias and dependence on data length relative to ApEn and better discriminated between regular and irregular dynamics, supporting its use for complexity analysis of physiological signals [6]. Book chapter by Akay.M [7], surveys nonlinear dynamic analysis for biomedical signals, including HRV, such as correlation dimension, Lyapunov exponents, fractal measures, and nonlinear time-series modelling. It argues that cardiovascular signals often exhibit nonlinear, possibly chaotic behavior and that nonlinear metrics may uncover subtle pathological alterations not detectable by linear analyses alone. Wavelet analysis captured dynamic, non-stationary modifications in HRV associated with ischaemia better than traditional Fourier methods, suggesting added value for detecting and characterizing ischaemic events [8]. Comprehensive survey of HRV analysis techniques (time-domain, frequency-domain, time–frequency, nonlinear/chaos, geometric) and clinical applications across cardiology, neurology, and psychiatry reported in [9]. A Kalman smoother–based algorithm by [10] to estimate time-varying HRV spectra, modelling RR-interval dynamics and recursively updating LF/HF components. This method provided smooth, high-resolution time courses of spectral components and outperformed sliding-window Fourier analysis in tracking rapid autonomic changes. Methodological guideline document describing measurement protocols, indices, and scoring rules for the Kardivar HRV system [11], including time- and frequency-domain metrics and composite stress indices. It establishes standardized procedures to quantify stress level and adaptive capacity, mapping numerical HRV indices to qualitative categories of autonomic regulation for screening and occupational/space-medicine applications.

GBD 2017 mortality and DALY/HALE [12 - 13] used standardized GBD models on global vital-registration, verbal-autopsy, and epidemiological data to estimate cause-specific deaths, DALYs, and healthy life expectancy for hundreds of diseases, showing declining age-standardized mortality but rising absolute deaths and DALYs dominated by non-communicable diseases and marked SDI-related inequalities. Stewart et al. [14] narratively reviewed US and European primary-prevention guidelines and major trials, concluding that absolute-risk–based intensive control of major risk factors plus strong population policies and lifestyle change are central, while evidence gaps persist for older, multimorbid, and real-world populations. Baevsky & Chernikova[15], briefly outlined HRV physiology and core time, spectral, geometric, and nonlinear methods, arguing that HRV indexes overall regulatory activity and reserves and must be interpreted under standardized, context-aware conditions. Singh et al., Schmidt et al., Mensah et al., and Castaldo et al., [16 – 19] collectively show that HRV and multimodal wearable data can prognosticate outcomes, guide training, and detect stress, that CVD remains the leading global killer, and that ultra-short HRV segments can approximate standard 5-min metrics for real-life mental-stress detection. TinyCare [20] runs compact ML models on microcontrollers to estimate blood pressure continuously from ECG/PPG, achieving clinically acceptable errors within very small memory and power budgets. TinyCES [21] deploys a CNN arrhythmia classifier on an Arduino-class device, reaches about 97% detection accuracy on MIT-BIH/PTB ECG data, and greatly cuts continuous data transmission. Tiny-PPG

[22] uses a lightweight deep network to detect motion artefacts in PPG on edge devices, attaining high segmentation accuracy with only tens of thousands of parameters and real-time execution on embedded hardware. Tsai et al.,[23] showed that PPG-derived HRV features combined with machine learning can quantify stress in real time with ECG-comparable accuracy, supporting unobtrusive mental-health monitoring. Strelchuk et al,.[24] demonstrated that HRV indices from PPG (e.g., SDNN, RMSSD) and classical classifiers reliably distinguish rest, stress, and recovery in a siren-based protocol. Behradfar et al.,[25] optimized mental-stress detection by selecting a compact HRV feature subset—especially normalized RR variability and LF power—that maintains high classification performance. Bahameish et al.,[26] proposed a robust HRV-based ML pipeline (segmentation, feature selection, careful validation) and found random forests most reliable for differentiating stress, neutral, and relaxation states. Pinge et al.,[27] reviewed wearable stress-detection studies, summarizing biosignals, features, and models, and emphasized gaps in real-world validation, dataset heterogeneity, and integration with intervention systems. In recent years, Photoplethysmography (PPG) has gained significant attention as a non-invasive and cost-effective alternative for cardiovascular monitoring. When HRV-related metrics are taken from PPG signals, the resulting measure is referred to as pulse rate variability (PRV). Several studies have proved a strong correlation between PRV and ECG-derived HRV under resting and low-motion cases, agreeing the feasibility of PPG-based stress assessment.

In this study, a broad stress detection framework based on multi-domain PRV analysis is proposed. Time-domain, frequency-domain, and nonlinear PRV features are derived from preprocessed PPG signals, and stress levels are calculated using the Baevsky Stress Index—a physiologically interpretable metric associated with sympathetic nervous system activation.

The main contributions of this paper are summarized as follows:

- A huge preprocessing and peak detection pipeline for reliable PRV extraction from noisy PPG signals.
- Comprehensive multi-domain PRV analysis incorporating time-domain, frequency-domain, and nonlinear features.
- Application of the Baevsky Stress Index for stress quantification using PPG-derived PRV.
- Validation of the proposed framework on publicly available datasets, showing a usability for wearable and edge-based healthcare systems.

The remainder of this research is organized as follows. Section 2 reviews related work on HRV- and PPG-based stress detection. Section 3 describes the proposed methodology. Section 4 presents experimental results and analysis. Section 5 discusses the findings and limitations, and Section 6 concludes the paper.

2. Related Work

Stress detection using physiological signals has been extensively studied because of its relevance in healthcare monitoring systems. ECG-based HRV analysis remains the gold standard for assessing autonomic regulation and stress response [15] [19]. Several studies have showed the effect of time-domain, frequency-domain, and nonlinear HRV features for stress classification using ECG signals. However, the reliance on electrode-based acquisition make an obstacle for scalability of such approaches for long-term monitoring. PPG-based stress detection has gained momentum with the proliferation of wearable devices. The WESAD dataset introduced a benchmark for multimodal stress detection, including PPG, ECG, electrodermal activity, and motion signals [17]. Subsequent studies have explored machine learning and deep learning approaches for stress classification using PPG signals [21 – 27]. While these methods often achieve high accuracy, they typically require complex models, large datasets, and extensive training, limiting interpretability and deployment on resource-constrained devices.

Geometric and statistical stress indices were obtained from HRV, such as the Baevsky Stress Index, offer physiologically interpretable measures of stress by quantifying sympathetic activation and variability reduction. Although widely applied in ECG-based studies, their use with PPG-derived PRV still relatively underexplored. More and more, existing work often focuses on single-domain analysis, which may not completely capture the complexity of autonomic dynamics. This research addresses these obstacles by integrating huge PPG preprocessing, multi-domain PRV analysis, and geometric stress index calculation into a unified and understandable framework.

Table 1. Related work comparisions

Study	Signal	Features	Dataset	Limitations
Castaldo et al.	ECG	HRV (Time/Freq)	Real-life	ECG-dependent
Schmidt et al.	PPG + ECG	ML-based	WESAD	Complex models
Tiny-PPG	PPG	CNN	ICU Data	Black-Box
This work	PPG	Multi-domain PRV + SI	WESAD+Physionet	Controlled Dataset

3. Materials and Methods

PhysioNet [28] is a publicly accessible online platform that grants access to an extensive compilation of recorded physiological signals. This comprehensive dataset repository encompasses cardiopulmonary, and additional biomedical signals derived from patients afflicted with diverse disease-related afflictions, as well as from other healthy patients. The first signal which we are using in here is Wearable Stress and Affect Detection Dataset [17]. This dataset with multiple modes consists of motion and physiological data that have been captured from both a device worn on the wrist and a device worn on the chest. The data was collected from 15 subjects who participated in a laboratory study. The dataset includes a number of sensor modalities, including body temperature, respiration, 3-axis acceleration, electrocardiogram, electromyogram, and pulse of blood volume. The second signal which we are using in here is Pulse Transit Time PPG Dataset from sensors which included the Electrocardiogram, Inertial, PPG, and Pressure sensors. The data was obtained from a group of 22 individuals who were in good health, and they performed three different physical activities during the recording sessions.

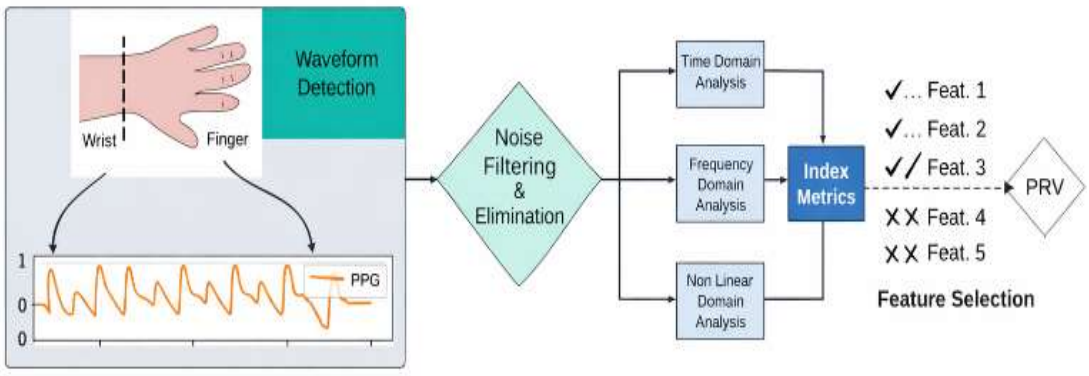

Figure 2. PPG Signal Processing and Feature Extraction Pipeline for PRV Analysis

Figure 2, illustrates the complete signal processing pipeline for deriving Pulse Rate Variability (PRV) from a Photoplethysmography (PPG) signal. PPG signals are acquired from peripheral measurement sites such as the wrist or finger, as shown in the initial block. The raw PPG waveform captures blood volume changes corresponding to cardiac cycles.

Following acquisition, the signal undergoes waveform detection, where the pulsatile component of the PPG signal is identified. The raw signal is then passed through a noise filtering and elimination stage to remove motion artifacts, baseline wander, and high-frequency noise, ensuring reliable pulse detection.

The preprocessed PPG signal is subsequently investigated across multiple domains:

- Time-domain analysis, which derives features related to pulse intervals and amplitude variations.
- Frequency-domain analysis, which captures spectral characteristics associated with autonomic nervous system activity.
- Non-linear domain analysis, which evaluates signal complexity and dynamical behavior.

According to these analyses, a set of index metrics (features) is computed. A feature selection step follows, where relevant features are retained and less informative or frequent features are discarded. The selected optimal feature subset is finally used to estimate Pulse Rate Variability (PRV), enabling physiological and cardiovascular assessments. Figure 3, illustrates the typical PPG signals with Systolic and Diastolic peaks. Figure 4 shows the cleaned PPG signals.

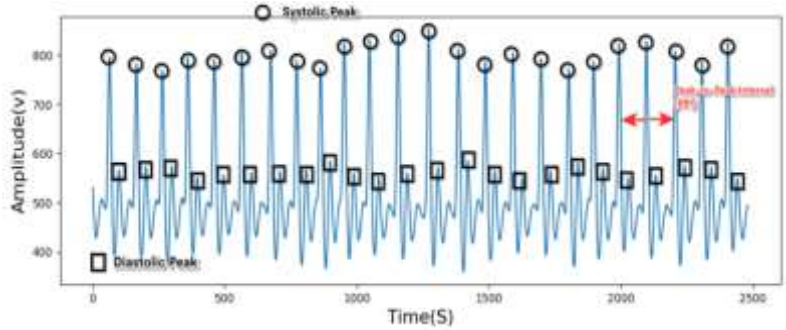

Figure 3. Typical PPG Signal Waveform

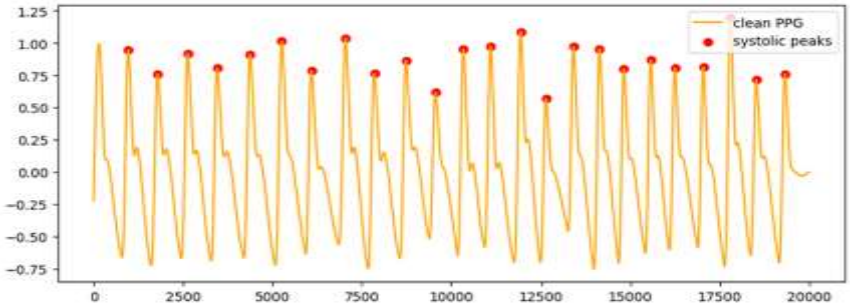

Figure 4. Cleaned PPG waveform

Algorithm 1: Peak Detection and IBI Extraction from PPG Signal

Input:

- Raw PPG signal S (sampled at fs Hz)
- Bandpass filter parameters: f_low = 0.5 Hz, f_high = 8 Hz, order = 4 (Butterworth)
- Refractory period: T_refract = 0.3 seconds (minimum time between successive peaks)

Output:

- Peak timestamps: T_peak = $\{t_1, t_2, \ldots, t_n\}$
- Inter-beat intervals: IBI = $\{IBI_1, IBI_2, \ldots, IBI_{n-1}\}$
- Heart rate: HR (beats per minute)

Procedure:

1. Preprocessing:

Remove NaN values and outliers from S
Apply 4th-order Butterworth bandpass filter [0.5–8 Hz] → filtered signal X
Compute adaptive threshold: Tp = μ(X) + 0.6 × σ(X), where μ and σ are mean and standard deviation of X

2. Peak Detection (local maxima with constraints):

Initialize empty peak list: P = []
Initialize last_peak_time = -∞
For i = 2 to length(X) - 1 do:
current_time = i / fs
If X(i) > Tp AND X(i) > X(i-1) AND X(i) > X(i+1) then:
(local maximum above threshold)
If (current_time - last_peak_time) ≥ T_refract then:
(satisfies refractory period)
Append (current_time, X(i)) to P
last_peak_time ← current_time
End If
End If
End For

3. IBI Computation and Artifact Rejection:

Extract timestamps: T_peak = $\{t_1, t_2, \ldots, t_n\}$ from P
For j = 1 to n-1 do:

IBI(j) = t(j+1) - t(j)
End For
Artifact rejection:
Remove IBI values outside physiological range [0.4 s, 2.0 s]
(corresponds to HR range 30–150 bpm)
Remove outliers: discard IBI(j) if |IBI(j) - median(IBI)| > 3 × MAD(IBI)
(MAD = median absolute deviation)
Retain cleaned IBI series: IBI_clean
4. Heart Rate Calculation:
HR = 60 / mean(IBI_clean)
Return: T_peak, IBI_clean, HR

3.1. PRV Analysis Methods

PRV is a physical event with different time intervals between each heartbeat. The difference in time between heartbeats contains detailed information about cardiovascular disease or chronic heart problems. The evaluation of HRV allows monitoring of the autonomic nervous system (ANS), which governs cardiac rhythm and indicates overall heart health. A healthy heart rate depends on the balanced interaction between the parasympathetic and sympathetic nervous systems. These systems, which function as the integral components of the ANS, must work together cohesively to achieve an optimal healthy state. The SNS is activated by sympathetic stimuli, such as stress, physical activity or heart disease. Some stimuli raise HR by causing the heart's sinoatrial node to fire more frequently and lowering heart rate variability. Internal organ function, allergic reactions, hemostasis maintenance, and the immune system are examples of parasympathetic processes that trigger the parasympathetic nervous system.

Within the low frequency range of 0.04 - 0.15 Hz, sympathetic activities and work are described. The higher frequency range of 0.15 Hz - 0.4 Hz is referred to in the parasympathetic exercises and activities[9,10], however numerous pathological conditions, including cardiovascular disease and stress, have an impact on heart rate and HRV. The central peripheral nervous systems also alter HRV maybe even severe brain damage or depression reduces the severity of cyclic changes in HR. The consistency of six HRV features (MeanNNI, StdNNI, MeanHR, StdHR, HF, SD1 and SD2) across different time lengths from 5 min to 1min was verified[19]. HRV metrics included normal-to-normal interval (NNI), HR, and High Frequency (HF) components. The analysis revealed that these short-term HRV features were effective for stress classification. Notably, HRV measurements taken for periods exceeding one minute demonstrated strong potential for automated mental stress detection.

3.1.1. Time Domain analysis

The signal is processed in the time domain. A peak detection algorithm is used to identify the peaks in the pre-processed and conditioned PPG waveform, which allows for real-time heart rate determination. Based on temporal variations, time domain analysis allows the identification and characterization of artifacts within PPG and ECG signals. Anomalies like abrupt spikes or irregularities can be found and eliminated during this analysis. Cleaned Signals are applied to consecutive RR interval cardiac values & are therefore the best to perform. The mean HR is the maximum intrusive level of this species. The overall diversity within the RR interval is measured by Standard Deviation of NN intervals (SDNN), which includes non-linearity in certain parameters.

Standard Deviation of Successive RR interval differences (SDSD) quantifies short-term heart rate variability by measuring the dispersion of differences between adjacent RR intervals and is defined as

$$\boldsymbol{SDSD} = \mathbb{E}\left\{\left(\Delta RR_j\right)^2\right\} - \left(\mathbb{E}\{\Delta RR_j\}\right)^2 \quad (1)$$

Where $\Delta RR_j = RR_{j+1} - RR_j$ denotes the difference between two successive RR intervals, and E{.} represents the expectation operator. In practice, SDSD is commonly expressed using root mean square of successive differences (RMSSD), which emphasis short term variability and parasympathetic activity, RMSSD is given by

$$\boldsymbol{RMSSD} = \sqrt{\frac{1}{N-1}\sum_{j=1}^{N-1}\left(RR_{j+1} - RR_j\right)^2} \quad (2)$$

Where N is the total number of RR intervals.

Another widely used time-domain metric is NN50, which counts the number of successive RR interval pairs that differ by more than 50 ms. Based on NN50, the pNN50 metric is defined as the percentage of such intervals relative to the total number of RR interval differences:

$$pNN50 = \frac{NN50}{N-1} \times 100\% \quad (3)$$

These time-domain metrics collectively provide valuable insight in to autonomic nervous system regulation and short-term heart rate variability analysis and the parameters are listed in Table 2.

Table 2. Time Domain Features

Parameter	Description
Avg	Average PP distance value
Var	PP's Variance
Median	PP's Median
Max	PP's Highest value
Min	PP's Lowest value
Range	The PP max-min range
RMSSD	The sum of squares differences between adjacent intervals divided by the square root of the mean
SDSD	The standard deviation of the variations among neighboring PP intervals
NNI - 50/20	The number of consecutive PP intervals with interval differences larger than 50 ms/20 ms
pNNI -50/20	The proportion derived by dividing I20(the number of interval differences of successive interval greater than 20ms)by the total number of PP intervals
Mean HR	The mean heart rate
Std HR	Standard Deviation of Heart Rate
Max HR	Maximum Heart Rate
Min HR	Minimum Heart Rate
Max NNI	The max of RR intervals
Min NNI	The min of RR intervals

3.1.2. Frequency Domain analysis

By breaking down/ segmenting a signal into its individual frequency components, frequency domain analysis makes it possible to identify artifacts. It is possible to isolate and reduce noise or interference at particular frequencies

The Power Spectrum Density (PSD) for the peak-to-peak interval series is approximated using this method. Prior to PSD estimation, the interval series is interpolated into an equidistant sampled collection since the general PSD estimators implicitly assume equidistant sampling. Fig 5 shows the Power spectral density of PPG signal. Table 3 lists the frequency domain features.

Short-term power spectrum analysis typically generates peaks or clusters of data points in three main areas :

- Vagus nerve and PNS activity are reflected by high frequency (HF) between 0.15 Hz and 0.40 Hz.
- SNS activity is reflected in the low frequency (LF) range of 0.04 Hz to 0.15 Hz.
- A number of factors are reflected in the very low frequency (VLF) of 0.003 Hz to 0.04 Hz, including not only the SNS, but also chemo or thermo-receptors the renin-angiotensin system, and Signal Processing methods.

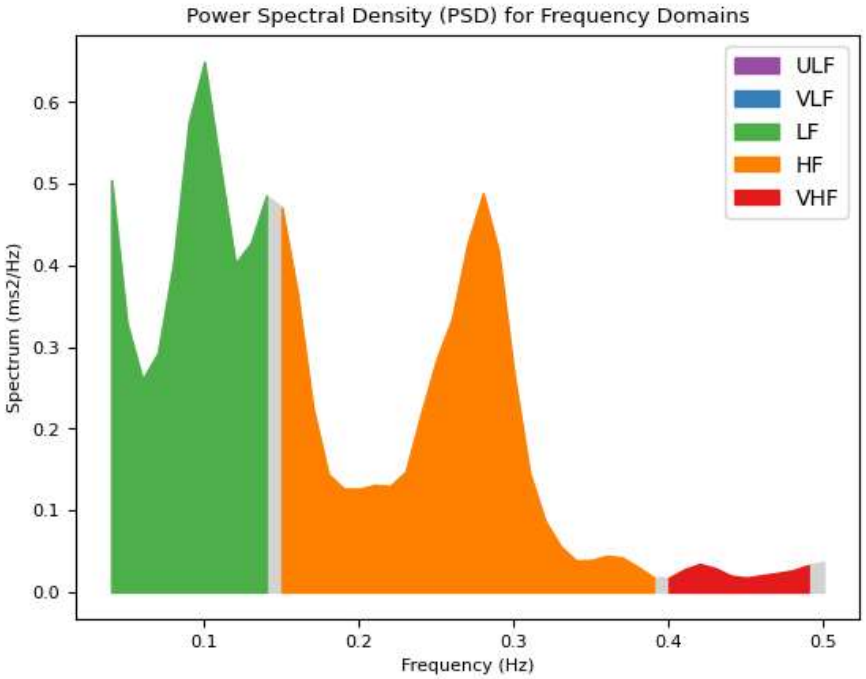

Figure 5. Power spectral density

Algorithm 2: Frequency-Domain PRV Feature Extraction

Input:

- Cleaned IBI series: IBI_clean = {IBI_1, IBI_2, …, IBI_m}
- Corresponding timestamps: T_IBI = {t_1, t_2, …, t_m}

Output:

- VLF power (ms^2), LF power (ms^2), HF power (ms^2), LF/HF ratio, Total Power (ms^2)

Procedure:

1. Interpolation to uniform sampling:

   Create uniform time grid: t_uniform = [T_IBI(1) : 0.25 : T_IBI(m)]

(4 Hz sampling, as recommended for HRV analysis)

   Apply cubic spline interpolation: IBI_interp = interp_cubic(T_IBI, IBI_clean, t_uniform)

   Detrend: IBI_detrend = IBI_interp - linear_trend(IBI_interp)

2. Power Spectral Density Estimation (Welch's method):

   Window: Hann window, length = 256 samples (64 seconds at 4 Hz)

   Overlap: 50% (128 samples)

   FFT length: 1024 points (zero-padded)

   Compute PSD: [PSD, freq] = welch(IBI_detrend, window, overlap, nfft, fs=4)

3. Frequency Band Power Integration:

   VLF band: 0.003–0.04 Hz

$VLF = \int_{0.003}^{0.04} PSD(f)\, df$ (trapezoidal integration)

   LF band: 0.04–0.15 Hz

$LF = \int_{0.04}^{0.15} PSD(f)\, df$

   HF band: 0.15–0.40 Hz

$HF = \int_{0.15}^{0.40} PSD(f)\, df$

   Total Power: 0.003–0.40 Hz

$TP = \int_{0.003}^{0.40} PSD(f)\, df$

   LF/HF ratio: LF_HF = LF / HF

4. Normalized Units (optional):

   LF_nu = LF / (LF + HF) × 100%

   HF_nu = HF / (LF + HF) × 100%

Return: {VLF, LF, HF, LF_HF, TP, LF_nu, HF_nu}

LF power reflects both sympathetic and parasympathetic modulation, while HF power primarily reflects parasympathetic (vagal) activity. The LF/HF ratio is commonly interpreted as an index of sympatho-vagal balance, with higher values indicating relative sympathetic dominance.

Table 3. Frequency Domain Features

Parameter	Description	Frequency Range
VLF	Very Low Frequency Power	0.003–0.04 Hz
LF	Low Frequency Power	0.04–0.15 Hz
HF	High Frequency Power	0.15–0.40 Hz
LF/HF	Ratio of LF to HF	—
Total Power	Total spectral power	0.003–0.40 Hz

3.1.3. Non-linear Domain analysis

Examining the cryptic, nonlinear relationships found in our data is the goal of nonlinear domain analysis. Artifacts that might follow nonlinear patterns can be accurately characterized using this technique.Nonlinear techniques are involved in HRV analysis because of the intricate control mechanisms.

Algorithm 3: Nonlinear PRV Feature Extraction

Input:

- Cleaned IBI series: IBI_clean = {IBI_1, IBI_2, …, IBI_m}

Output:

- Poincaré plot metrics: SD1, SD2, SD1/SD2 ratio, SD1×SD2 (ellipse area)
- Entropy metrics: ApEn, SampEn

Procedure:

A. Poincaré Plot Analysis:

1.Construct Poincaré plot: For each j = 1 to m-1, plot point (IBI(j), IBI(j+1))

2.Compute successive differences: ΔIBI(j) = IBI(j+1) - IBI(j)

3.SD1 (short-term variability, perpendicular to identity line):

SD1 = $\sqrt{(Var(\Delta IBI) / 2)} = \sqrt{(½\ SDSD^2)}$

4.SD2 (long-term variability, along identity line):

SD2 = $\sqrt{(2\times SDNN^2 - ½\times SDSD^2)}$

where SDNN = standard deviation of IBI_clean,

SDSD = standard deviation of ΔIBI

5.Derived metrics:

SD1/SD2 ratio (quantifies balance between short- and long-term variability)

SD1×SD2 (area of fitted ellipse)

B. Approximate Entropy (ApEn):

Parameters: - Embedding dimension: m = 2 - Tolerance: r = 0.2 × SD(IBI_clean) - Sequence length: N = length(IBI_clean)

Computation: - Form m-dimensional vectors: U(i) = {IBI(i), IBI(i+1), …, IBI(i+m-1)} for i = 1 to N-m+1 - For each U(i), count matches: $C_i^m(r)$ = (number of U(j) where distance(U(i), U(j)) ≤ r) / (N - m + 1)

Compute: $\varphi^m(r) = (1/(N-m+1)) \Sigma \log(C_i^m(r))$

Repeat for (m+1)-dimensional vectors to get $\varphi^{m+1}(r)$ - ApEn(m, r, N) = $\varphi^m(r) - \varphi^{m+1}(r)$

C. Sample Entropy (SampEn):

Parameters: Same as ApEn (m = 2, r = 0.2 × SD(IBI_clean))

Computation: - Form vectors as in ApEn, but exclude self-matches - For each U(i), count matches: $B_i^m(r)$ for m-dimensional and $A_i^m(r)$ for (m+1)-dimensional - SampEn(m, r, N) = $-\log(\Sigma A_i^m(r) / \Sigma B_i^m(r))$

Interpretation: - Lower entropy values → more regular, predictable signal (reduced complexity) - Higher entropy values → more irregular, complex signal - During stress, entropy typically decreases due to reduced variability and parasympathetic withdrawal

Return: {SD1, SD2, SD1/SD2, SD1×SD2, ApEn, SampEn}

In the above algorithm, all nonlinear metrics are computed on the IBI time series, not on the raw PPG waveform.

Methods like the Poincaré diagram, analyze the non-linear HRV features which can be examined using recurrence plots, correlation dimension, detrended fluctuation analysis, and approximate and

sample entropy [15]. The drawback of these methods remains the challenge of explaining the results physiologically.One of the most widely used nonlinear techniques, the Poincaré Plot, is distinguished by a graphical depiction of the correlation between successive RR intervals and permits simple interpretation. i.e.. a plot of RRj+1 [14,15], as a function of RRj. This relation is described by the following fig.6 and the parameters are listed in Table 4.

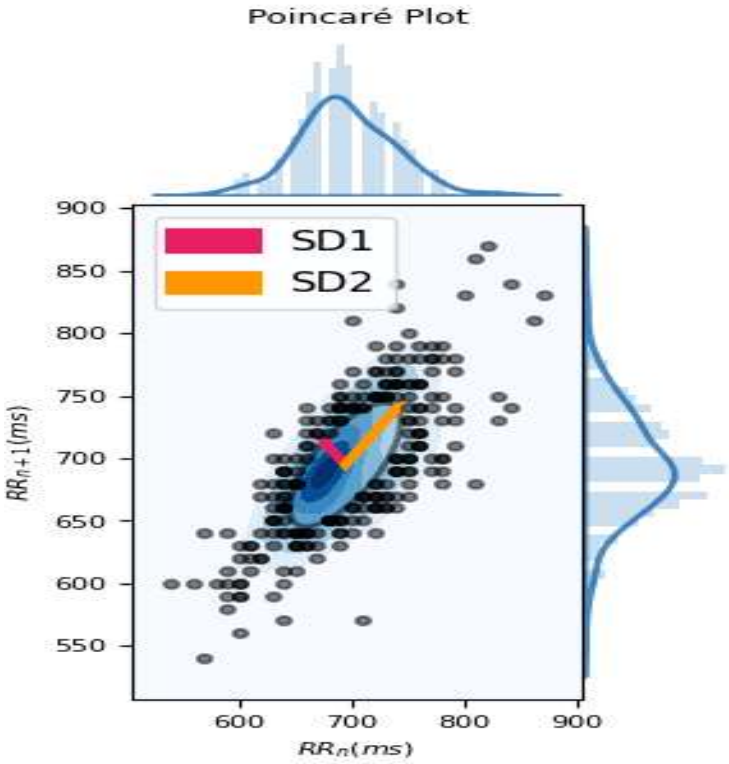

Figure 6. Poinclare plot

Table 4. Poincaré and Nonlinear Features

Parameter	Description
SD1	Standard deviation perpendicular to the line of identity in Poincaré plot (short-term variability)
SD2	Standard deviation along the line of identity in Poincaré plot (long-term variability)
SD1/SD2	Ratio quantifying balance between short- and long-term variability
SD1×SD2	Area of fitted ellipse in Poincaré plot
ApEn	Approximate Entropy (m=2, r=0.2×SD); measures signal regularity
SampEn	Sample Entropy (m=2, r=0.2×SD); improved version of ApEn with reduced bias

The SD of each point perpendicular to the identity line, which connects the short-term variability primarily caused by RSA, is represented by SD1. The time domain measure SDSD is used to represent SD1. which is:

$$SD1^2 = \frac{1}{2SDSD^2} \quad (4)$$

SD2 is the standard deviation across the identity line that measures long-term variability in the time domain measurements SDNN and SDSD.

$$SD_2^2 = 2SD_{NN}^2 - SDSD^2 \quad (5)$$

4. Results and Discussion

4.1. Experimental Setup

Our proposed method was validated using the Pulse Transit Time PPG Dataset and the Wearable Stress and Affect Detection (WESAD) public dataset.

4.1.1. Dataset Description and Labeling

WESAD Dataset:

The Wearable Stress and Affect Detection (WESAD) dataset [17] contains multimodal physiological data from 15 subjects (12 male, 3 female, age 27.5 ± 2.4 years) collected during a laboratory stress-induction protocol. Each subject underwent:

- Baseline condition: 20-minute seated rest with eyes closed
  Used for analysis: 18 minutes (discarded first 2 minutes for physiological settling)
- Stress condition: Trier Social Stress Test (TSST) protocol (10 minutes total)
  Public speaking preparation (2 min) → excluded
  Public speaking task (5 min) → included
  Mental arithmetic task (3 min) → included
  Total used: 8 minutes

PPG signal was acquired from a chest-worn device (RespiBAN) at 64 Hz sampling rate. Binary labels were extracted from the original dataset annotation: 0 = baseline, 1 = stress.

PTT Dataset:

The Pulse Transit Time PPG dataset contains signals from 22 healthy subjects performing physical activities. For this study, we used only the resting/seated segments (total ~15 minutes per subject) as additional baseline validation data. PPG was sampled at 125 Hz. This dataset was not used for stress classification, only for validating feature stability. This section may be divided by subheadings. It should provide a concise and precise description of the experimental results, their interpretation, as well as the experimental conclusions that can be drawn.

4.1.2. Windowing and Data Partitioning

Window construction: Primary window length: 5 minutes (300 seconds), non-overlapping. Additional window lengths: 1, 2, 3, and 4 minutes (for feature stability analysis). Transition exclusion: First 2 minutes after each condition change were discarded

WESAD windowing: Baseline (18 min) → 3 non-overlapping 5-min windows per subject. Stress (8 min) → 1 non-overlapping 5-min window per subject (starting at minute 3). Total: 15 subjects × (3 baseline + 1 stress) = 60 windows (45 baseline, 15 stress)

Subject-wise train-test split: Training set: 10 subjects → 30 baseline + 10 stress = 40 windows .Test set: 5 subjects → 15 baseline + 5 stress = 20 windows. No subject appears in both training and test sets.

4.1.3. Statistical Analysis

Tests: Normality assessment: Shapiro-Wilk test (α = 0.05). Parametric test: Paired t-test (if normality satisfied). Non-parametric test: Wilcoxon signed-rank test (if normality violated). Multiple comparison correction: Bonferroni correction for 17 tested features (adjusted α = 0.05/17 = 0.0029). Effect size: Cohen's d for paired samples

Correlation analysis:

To assess feature stability across window lengths, Pearson correlation coefficient (R^2) was computed between features extracted from 5-minute windows and features from shorter windows (1, 2, 3, 4 min), pooled across all subjects. Features with $R^2 \geq 0.6$ for at least three shorter window lengths were retained as "stable" features.

Comparison of the PRV parameters for Normal and Stressed Conditions are given in fig 7. and R^2 Values for certain parameters are provided in table 5.

Table 5. Correlation (R^2) of PRV Features Across Window Lengths

PRV Feature	1-min	2-min	3-min	4-min	Retained
Mean HR	0.92	0.95	0.97	0.98	✓
Min HR	0.90	0.93	0.95	0.96	✓
Max HR	0.88	0.91	0.94	0.96	✓
Mean NNI	0.97	0.98	0.99	0.99	✓
Median NNI	0.96	0.97	0.98	0.99	✓
Max NNI	0.93	0.95	0.97	0.98	✓

Min NNI	0.87	0.90	0.93	0.95	✓
SDNN	0.72	0.81	0.88	0.92	✓
RMSSD	0.88	0.92	0.95	0.97	✓
SDSD	0.88	0.91	0.94	0.96	✓
pNN50	0.76	0.85	0.90	0.93	✓
pNN20	0.54	0.62	0.68	0.72	✗
LF power	0.65	0.74	0.82	0.88	✓
HF power	0.62	0.71	0.79	0.85	✓
LF/HF ratio	0.58	0.68	0.75	0.81	✓
SD1	0.88	0.92	0.95	0.97	✓
SD2	0.73	0.82	0.89	0.93	✓
SampEn	0.61	0.70	0.77	0.83	✓
ApEn	0.59	0.68	0.75	0.81	✓
VLF power	0.38	0.45	0.52	0.58	✗
Total Power	0.47	0.56	0.64	0.71	✗
Var NNI	0.51	0.60	0.68	0.74	✗

In the above table, features with $R^2 \geq 0.6$ in at least three window lengths were retained for subsequent analysis. Four features (pNN20, VLF power, Total Power, Var NNI) did not meet the stability criterion and were excluded.

An inaccurate duration between consecutive peaks is present due to the inability to perfectly extract all the points of the signal. Consequently, intervals that deviate by approximately 250-300ms more or less than the average of all the intervals are excluded, while the remaining intervals are employed for the extraction of HRV. Several additional factors are also taken into account to assess the index, such as high-frequency power and the RMSSD (Root Mean Square of Sequential R-interval Difference).

4.1.4. PRV Feature Comparison Between Stress and Baseline

Table 6, presents descriptive statistics for selected PRV features under baseline and stress conditions, along with statistical test results.

Table 6. PRV Features in Baseline vs Stress Conditions

PRV Feature	Baseline (Mean ± SD)	Stress (Mean ± SD)	Test Statistic	p-value	Cohen's d
Mean HR (bpm)	71.2 ± 9.8	86.5 ± 11.2	t(14) = -9.32	< 0.001*	2.41
Mean NNI (ms)	858.3 ± 118.5	712.4 ± 95.7	t(14) = 8.91	< 0.001*	1.35
SDNN (ms)	65.3 ± 12.4	42.7 ± 9.8	t(14) = 8.45	< 0.001*	2.01
RMSSD (ms)	54.2 ± 10.1	31.8 ± 7.5	t(14) = 10.12	< 0.001*	2.54
pNN50 (%)	35.6 ± 8.2	18.3 ± 6.7	t(14) = 9.78	< 0.001*	2.32
LF power (ms^2)	1245 ± 320	1890 ± 410	t(14) = -6.21	< 0.001*	1.75
HF power (ms^2)	1120 ± 280	680 ± 190	t(14) = 7.83	< 0.001*	1.88
LF/HF ratio	1.11 ± 0.28	2.78 ± 0.62	W = 0†	< 0.001*	3.42
SD1 (ms)	38.3 ± 7.1	22.5 ± 5.3	t(14) = 10.34	< 0.001*	2.56
SD2 (ms)	87.2 ± 16.9	58.9 ± 13.2	t(14) = 8.02	< 0.001*	1.85
ApEn	1.22 ± 0.15	0.98 ± 0.12	t(14) = 6.87	< 0.001*	1.77
SampEn	1.68 ± 0.22	1.37 ± 0.18	t(14) = 5.92	< 0.001*	1.53

*Bonferroni-corrected threshold: $p < 0.0029$

†Wilcoxon signed-rank test used (non-normal distribution); W = sum of positive ranks

Interpretation:

Time-domain metrics: Significant reductions in SDNN, RMSSD, and pNN50 during stress indicate decreased overall heart rate variability and reduced parasympathetic (vagal) activity. The large effect sizes (Cohen's d > 2.0) confirm robust physiological responses to the TSST stressor.

Frequency-domain metrics: The increase in LF power and decrease in HF power during stress resulted in a significant elevation of the LF/HF ratio (1.11 → 2.78, $p < 0.001$), consistent with sympathetic nervous system dominance and parasympathetic withdrawal. This pattern is well-established in stress physiology literature [4, 15].

Nonlinear metrics: Reductions in ApEn and SampEn during stress indicate decreased complexity and increased regularity in heart rate dynamics. Similarly, decreases in SD1 and SD2 (Poincaré plot) reflect reduced short- and long-term variability, respectively. These findings align with the known effects of sympathetic activation on cardiac rhythm.

Comparision of Baevsky Stress Index results for baseline and stress condition is given in Table 7.

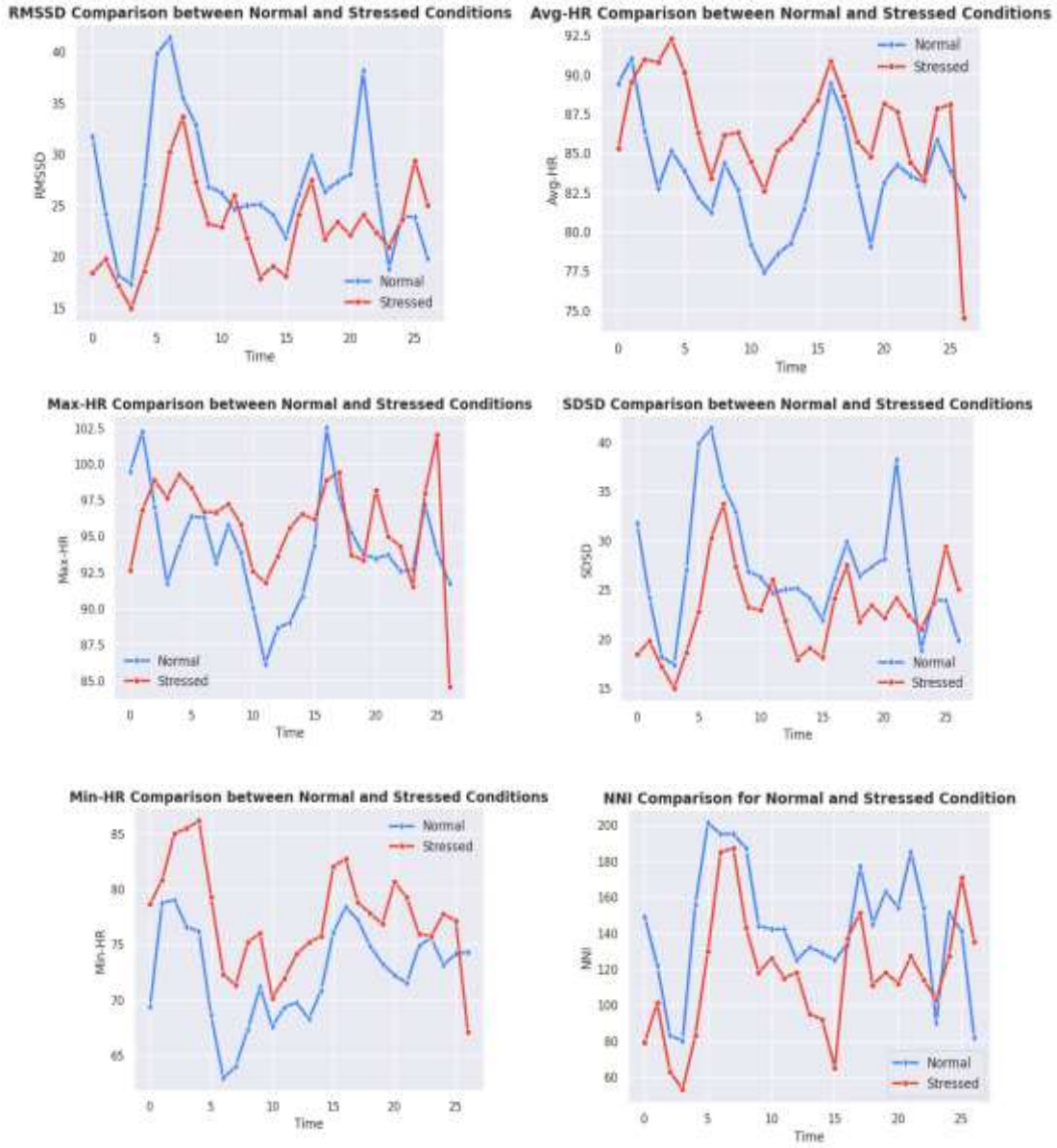

Figure 7. Stress comparison charts of parameters

Table 7. Baevsky Stress Index Comparison

Condition	Mean SI ± SD	Range	Interpretation
Baseline	2.1 ± 0.8	0.9 – 4.7	Normal regulatory state
Stress	6.8 ± 1.9	4.2 – 11.3	Moderate to high stress

Reference ranges (Baevsky [11]): SI < 50: Normal, good adaptation. SI 50–150: Moderate stress, adaptive strain. SI 150–500: High stress, regulatory failure .SI > 500: Severe exhaustion. In our experimentation, the SI values in this study (0.9–11.3) are considerably lower than classical Baevsky reference ranges, likely due to: 1. Differences in RR-interval histogram bin width (we used 20 ms; classical method uses 50 ms) 2. Short-duration laboratory stress vs chronic occupational/space-mission stress in original Baevsky studies 3. Young healthy cohort with strong adaptive capacity. Despite absolute scale differences, the relative change (3.2-fold increase from baseline to stress) is physiologically meaningful and consistent across subjects.

4.2. Discussion

4.2.1. Physiological Interpretation

The observed PRV feature changes during the TSST-induced stress condition are consistent with established autonomic nervous system physiology. Stress activates the sympathetic branch of the ANS, leading to:

1. Increased heart rate (Mean HR: 71.2 → 86.5 bpm), mediated by β-adrenergic stimulation of the sinoatrial node
2. Reduced variability (SDNN, RMSSD, pNN50 all decreased), reflecting parasympathetic withdrawal and reduced respiratory sinus arrhythmia
3. Shifted spectral balance (LF/HF ratio: 1.11 → 2.78), indicating relative sympathetic dominance
4. Decreased complexity (ApEn, SampEn, SD1, SD2 reduced), consistent with loss of vagal modulation and more rigid, stereotyped cardiac control

The Baevsky Stress Index showed a 3.2-fold increase during stress (2.1 → 6.8), confirming its sensitivity to acute psychological stressors in laboratory settings.

4.2.2. PPG-Based PRV vs ECG-Based HRV

Our results demonstrate that PPG-derived PRV metrics, particularly **time-domain** features (SDNN, RMSSD, Mean HR, pNN50) and Poincaré plot features (SD1, SD2), can reliably capture stress-induced autonomic changes. This is consistent with prior work [19, 23, 24] showing strong agreement between PPG-PRV and ECG-HRV under resting and controlled conditions.

Frequency-domain features (LF, HF, LF/HF) also showed significant stress-baseline differences, though their absolute values may differ from ECG-based measurements due to pulse transit time effects and peripheral vascular modulation. The directional change (increased LF/HF during stress) remains physiologically valid and supports the use of PPG for autonomic assessment in wearable applications

4.2.3. Feature Stability Across Window Lengths

Table 5 and Figure 7 demonstrate that most PRV features maintain strong correlation ($R^2 \geq 0.6$) with 5-minute reference values when computed from windows as short as 2–3 minutes. This suggests feasibility for near-real-time stress monitoring applications where 5-minute stationary recordings are impractical.

Features with highest stability ($R^2 > 0.90$ across all window lengths): Mean HR, Mean NNI, Median NNI, Max NNI, RMSSD, SDSD, SD1.

Features with moderate stability (R^2 0.60–0.80 for shorter windows): SDNN, pNN50, LF power, HF power, SampEn, ApEn.

5. Limitations of the study

1. Laboratory-induced stress: The TSST protocol induces acute psychological stress in a controlled setting, which may not fully represent chronic real-world stressors (work pressure, social conflict, and environmental factors).
2. Sample size: 15 subjects (WESAD) limits statistical power for subgroup analysis and generalizability across populations.
3. Motion artifacts: Both datasets involved seated or low-activity conditions. Performance under ambulatory or high-motion scenarios requires further validation.
4. Frequency-domain reliability: PPG-based LF and HF power estimates are influenced by pulse transit dynamics and peripheral vascular tone, which may introduce additional variability compared to ECG-based measurements.
5. Single-modality focus: This study analyzed PPG-PRV features exclusively. Integration with other wearable signals (electrodermal activity, respiration, accelerometry) may improve stress detection accuracy and will be explored in future work.
6. Recent papers [29 -30] have explored the HRV analysis through machine learning techniques and reported a good F1 score of 95%, we are yet to explore the Deep learning and Machine learning techniques and reserved for our future work.

5.1. Practical Implications

The validated PRV feature set and processing pipeline enable: - Wearable stress monitoring using low-cost PPG sensors (widely available in smartwatches and fitness trackers) - Edge-device

implementation due to computational simplicity (no deep learning inference required for feature extraction) - Near-real-time assessment with window lengths as short as 2–3 minutes.

Future work will focus on: Development and validation of machine learning classification models using the extracted PRV features. Multimodal fusion with EDA, respiration, and activity signals. Real-world validation in ambulatory and occupational settings. Personalized stress detection algorithms accounting for individual baseline variability.

6. Conclusions

This study presented a comprehensive framework for extracting and validating multi-domain Pulse Rate Variability (PRV) features from photoplethysmography (PPG) signals for stress detection. Using the WESAD and PTT datasets, we demonstrated that:

1. Proper peak detection with refractory constraints and artifact rejection is essential for reliable IBI extraction from PPG signals.
2. Time-domain PRV features (SDNN, RMSSD, pNN50, Mean HR) show significant and large-effect differences between baseline and stress conditions ($p < 0.001$, Cohen's $d > 1.5$), supporting their utility for autonomic assessment.
3. Frequency-domain features (LF power, HF power, LF/HF ratio) capture the shift toward sympathetic dominance during stress, though absolute values may differ from ECG-based measures.
4. Nonlinear features (ApEn, SampEn, Poincaré SD1/SD2) provide additional sensitivity to changes in cardiac rhythm complexity.
5. The Baevsky Stress Index, adapted for PPG-PRV, shows a consistent 3.2-fold increase during laboratory-induced stress.
6. Most PRV features exhibit strong stability ($R^2 \geq 0.6$) across window lengths from 2–5 minutes, enabling near-real-time applications.

These findings confirm the feasibility of PPG-based, multi-domain PRV analysis as a non-invasive, wearable-compatible approach for stress assessment. Future work will develop machine learning classification models, validate the framework in real-world ambulatory settings, and explore multimodal physiological integration to enhance stress detection accuracy and robustness.

Funding: This work was supported by "The Deanship of Scientific Research, Vice-Presidency for Graduate Studies and scientific Research, King Faisal University, Ministry of Education, Saudi Arabia under Grant KFU254707".

Data Availability Statement: The WESAD and PPG datasets were used for the study. The Methodology and materials, algorithm, experimental setting discussed in this work would enable the reader to reproduce the result.

Acknowledgments: Authors acknowledge "The Deanship of Scientific Research, Vice-Presidency for Graduate Studies and scientific Research, King Faisal University, Ministry of Education, Saudi Arabia under Grant KFU254707.

Conflicts of Interest: The authors declare no conflict of interest.

References

1. Solange Akselrod et al. ,Power Spectrum Analysis of Heart Rate Fluctuation: A Quantitative Probe of Beat-to-Beat Cardiovascular Control.Science213,220-222(1981).DOI:10.1126/science.6166045.
2. Hirsch, J. A., & Bishop, B. Respiratory sinus arrhythmia in humans: how breathing pattern modulates heart rate. The American journal of physiology,241(4)(1981). https://doi.org/10.1152/ajpheart.1981.241.4.H620.
3. Pomeranz, B., Macaulay, R. J., Caudill, M. A., Kutz, I., Adam, D., Gordon, D., Kilborn, K. M., Barger, A. C., Shannon, D. C., & Cohen, R. J. (1985). Assessment of autonomic function in humans by heart rate spectral analysis. The American journal of physiology, 248. https://doi.org/10.1152/ajpheart.1985.248.1.H15.
4. Pagani, M., Lombardi, F., Guzzetti, S., Rimoldi, O., Furlan, R., Pizzinelli, P., Sandrone, G., Malfatto, G., Dell'Orto, S., & Piccaluga, E. (1986). Power spectral analysis of heart rate and arterial pressure variabilities as a marker of sympatho-vagal interaction in man and conscious dog. Circulation research, 59(2), 178–193. https://doi.org/10.1161/01.res.59.2.178.
5. Woo, M.A., Stevenson, W.G., Moser, D.K., Trelease, R.B. and Harper, R.M., 1992. Patterns of beat-to-beat heart rate variability in advanced heart failure. American heart journal, 123(3), pp.704-710.
6. Richman, J.S. and Moorman, J.R., 2000. Physiological time-series analysis using approximate entropy and sample entropy. American Journal of Physiology-Heart and Circulatory Physiology, 278(6), pp.2039-2049.
7. Akay, M., Nonlinear biomedical signal processing dynamic analysis and modeling, vol II, Wiley(2001) , pp. 133-213.
8. Gamero, L.G., Vila, J. and Palacios, F., Wavelet transform analysis of heart rate variability during myocardial ischaemia. Medical and Biological Engineering and Computing, 40(1),2002, pp.72-78.
9. U.R. Acharya, K.P. Joseph, N. Kannathal, C.M. Lim, and J.S. Suri. Heart rate variability: a review. Med Biol Eng Comput, 44:1031–1051, 2006.
10. Tarvainen M, Georgiadis S, Karjalainen P. Time-varying analysis of heart rate variability with kalman smoother algorithm. Conf Proc IEEE Eng Med Biol Soc. 2005;2005:2718-21. doi: 10.1109/IEMBS.2005.1617032. PMID: 17282801.
11. Baevsky, R. M., & Chernikova, A. G. Heart Rate Variability Analysis: Physiological Foundations and Main Methods. Cardiometry, 10, 2017,66-76. doi:10.12710/cardiometry.2017.10.6676
12. GBD 2017 Causes of Death Collaborators. Global, regional, and national age-sex-specific mortality for 282 causes of death in 195 countries and territories, 1980-2017: a systematic analysis for the Global Burden of Disease Study 2017. Lancet. 2018 Nov 10;392(10159):1736-1788. doi: 10.1016/S0140-6736(18)32203-7. Epub 2018 Nov 8.
13. GBD 2017 DALYs and HALE Collaborators.Global, regional, and national disability-adjusted life-years (DALYs) for 359 diseases and injuries and healthy life expectancy (HALE) for 195 coun-tries and territories, 1990-2017: a systematic analysis for the Global Burden of Disease Study2017. Lancet 2018;392:1859–922.
14. Stewart J, Manmathan G, Wilkinson P. Primary prevention of cardiovascular disease: A review of contemporary guidance and literature. JRSM Cardiovascular Disease. 2017;6. doi:10.1177/2048004016687211.
15. Baevsky,R.M.;Chernikova,A.G.Heart Rate Variability Analysis:Physiological Foundations And Main Methods.Cardiometry 2017, 10,66–67.
16. Singh N, Moneghetti KJ, Christle JW, Hadley D, Froelicher V, Plews D. Heart Rate Variability: An Old Metric with New Meaning in the Era of Using mHealth technologies for Health and Exercise Training Guidance. Part Two: Prognosis and Training. Arrhythm Electrophysiol Rev. 2018 Dec;7(4):247-255. doi: 10.15420/aer.2018.30.2. PMID: 30588312; PMCID: PMC6304793.
17. Philip Schmidt, Attila Reiss, Robert Duerichen, Claus Marberger, and Kristof Van Laerhoven. 2018. Introducing WESAD, a Multimodal Dataset for Wearable Stress and Affect Detection. In Proceedings of the 20th ACM International Conference on Multimodal Interaction (ICMI '18). Association for Computing Machinery, New York, NY, USA, 400–408. https://doi.org/10.1145/3242969.3242985.
18. Mensah, G, Roth, G, Fuster, V. The Global Burden of Cardiovascular Diseases and Risk Factors: 2020 and Beyond. J Am Coll Cardiol. 2019 Nov, 74 (20) 2529–2532.
19. Castaldo, R., Montesinos, L., Melillo, P. et al. Ultra-short term HRV features as surrogates of short term HRV: a case study on mental stress detection in real life. BMC Med Inform Decis Mak 19, 12 (2019). https://doi.org/10.1186/s12911-019-0742-y.
20. K. Ahmed and M. Hassan, "tinyCare: A tinyML-based Low-Cost Continuous Blood Pressure Estimation on the Extreme Edge," 2022 IEEE 10th International Conference on Healthcare Informatics (ICHI), Rochester, MN, USA, 2022, pp. 264-275, doi: 10.1109/ICHI54592.2022.00047.

21. Kim, E., Kim, J., Park, J., Ko, H., & Kyung, Y. (2023). TinyML-Based Classification in an ECG Monitoring Embedded System. Computers, Materials and Continua, 75(1), 1751-1764.
22. Yali Zheng, Chen Wu, Peizheng Cai, Zhiqiang Zhong, Hongda Huang, Yuqi Jiang, Tiny-PPG: A lightweight deep neural network for real-time detection of motion artifacts in photoplethysmogram signals on edge devices, Internet of Things, Vol.25,2024,101007,ISSN 2542-6605, https://doi.org/10.1016/j.iot.2023.101007.
23. Tsai YY, Chen YJ, Lin YF, Hsiao FC, Hsu CH, Liao LD. Photoplethysmography-based HRV analysis and machine learning for real-time stress quantification in mental health applications. APL Bioeng. 2025 Apr 3;9(2):026103. doi: 10.1063/5.0256590. PMID: 40191605; PMCID: PMC11970940.
24. Yaroslav Strelchuk, Alina Nechyporenko, Marcus Frohme, Vitaliy Gargin, Andrii Lupyr, Victoriia Alekseeva. Detection of Stress Using Photoplethysmography. 2024, 7th International Conference on Informatics & Data-Driven Medicine.pp.196-202,Vol.3892.
25. Behradfar, M., Roy, S., & Nuamah, J. (2025). Optimizing Mental Stress Detection via Heart Rate Variability Feature Selection. Sensors, 25(13), 4154. https://doi.org/10.3390/s25134154.
26. Bahameish M, Stockman T, Requena Carrión J. Strategies for Reliable Stress Recognition: A Machine Learning Approach Using Heart Rate Variability Features. Sensors (Basel). 2024 May 18;24(10):3210. doi: 10.3390/s24103210. PMID: 38794064; PMCID: PMC11126126.
27. Pinge, Anuja, et al. "Detection and Monitoring of Stress Using Wearables: A Systematic Review." Frontiers in Computer Science, vol. 6, 2024, p. 1478851, https://doi.org/10.3389/fcomp.2024.1478851.
28. Goldberger AL, Amaral LAN, Glass L, Hausdorff JM, Ivanov PCh, Mark RG, Mietus JE, Moody GB, Peng C-K, Stanley HE. PhysioBank, PhysioToolkit, and PhysioNet: Components of a New Research Resource for Complex Physiologic Signals. Circulation 101(23):e215-e220.
29. Behradfar M, Roy S, Nuamah J. Optimizing Mental Stress Detection via Heart Rate Variability Feature Selection. Sensors (Basel). 2025 Jul 3;25(13):4154. doi: 10.3390/s25134154. PMID: 40648409; PMCID: PMC12252238.
30. Ranjan, V.; Singh, R.; Ganguly, A.; Halder, S. Detecting Meditative States Through Heart Rate Variability and Machine Learning Techniques. Proceedings of 5th International Conference on Frontiers in Computing and Systems, 2026. pp. 563–575. https://doi.org/10.1007/978-981-96-8309-3_39.